# Drop impact into a deep pool: vortex shedding and jet formation

**G. Agbaglah[1]†, M.-J. Thoraval[2,3], S. T. Thoroddsen[2], L. V. Zhang[1], K. Fezzaa[4], R. D. Deegan[1]‡**

[1]Department of Physics and Center for the Study of Complex Systems, University of Michigan, Ann Arbor, Michigan 48109, USA

[2]Division of Physical Sciences and Engineering & Clean Combustion Research Center, King Abdullah University of Science and Technology (KAUST), Thuwal, 23955-6900, Saudi Arabia

[3]Physics of Fluids Group, Faculty of Science and Technology, Mesa+ Institute, University of Twente, 7500 AE Enschede, The Netherlands

[4]X-Ray Science Division, Argonne National Laboratory, Argonne, IL 60439, USA

(Received 5 December 2014)

One of the simplest splashing scenarios results from the impact of a single drop on a deep pool. The traditional understanding of this process is that the impact generates an axisymmetric sheet-like jet that later breaks up into secondary droplets. Recently it was shown that even this simplest of scenarios is more complicated than expected because multiple jets can be generated from a single impact event and there are transitions in the multiplicity of jets as the experimental parameters are varied. Here we use experiments and numerical simulations of a single drop impacting on a deep pool to examine the transition from impacts that produce a single jet to those that produce two jets. Using high speed X-ray imaging methods we show that vortex separation within the drop leads to the formation of a second jet long after the formation of the ejecta sheet. Using numerical simulations we develop a phase diagram for this transition and show that the capillary number is the most appropriate order parameter for the transition.

**Key words:** breakup/coalescence, drops

## 1. Introduction

Drop impact phenomena are omnipresent in nature and industrial applications. Despite well over a hundred years of study many fundamental questions - regarding, for example, splash morphology, droplet size distribution, merger process of the drop and liquid substrate - remain unsettled (Yarin 2006; Deegan *et al.* 2008). An ongoing renaissance of the subject driven by new experimental (Thoroddsen *et al.* 2003; Xu *et al.* 2005; Fezzaa & Wang 2008; Kolinski *et al.* 2012) and computational techniques (Oguz & Prosperetti 1989; Josserand & Zaleski 2003; Popinet 2003; Howison *et al.* 2005; Popinet 2009; Tryggvason *et al.* 2011) has revealed previously unsuspected effects and structures. One such structure is the *ejecta sheet*.

From Worthington's pioneering studies (Worthington 1882) onward the standard picture of splashing from drop impact with a liquid layer consisted of the formation, growth, and disintegration of a single sheet-like jet, herein called the lamella. However, Weiss &

† Email address for correspondence: agbagla@umich.edu
‡ Email address for correspondence: rddeegan@umich.edu

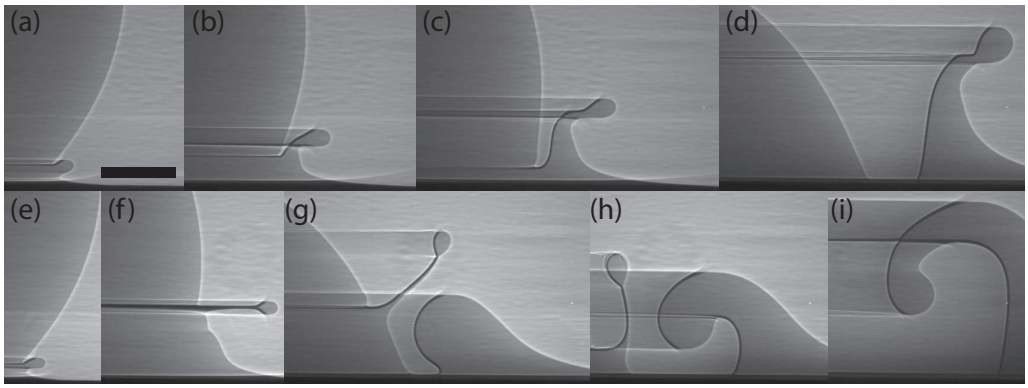


FIGURE 1. Phase contrast X-ray images showing the evolution of the lamella (a-d) at $We = 268$ and $Re = 1978$ and an ejecta sheet and roll jet (e-i) at $We = 292$ and $Re = 2042$. At later times (not shown) the tip of the roll jet overtakes the base, and the jet curves away from the center rather than as shown in (g-i) where it curves towards the center. The scale bar correspond to 0.25 mm. Time increases from left to right.

Yarin (1999) using inviscid irrotational numerical computations found evidence of an earlier jet but did not follow its evolution through the entire lifetime of the splash, because of a very strong stretching of the Lagrangian frame they used. This jet was first observed experimentally by Thoroddsen (2002), who called it the ejecta sheet, though his experiments revealed that the ejecta sheet evolved into the leading edge of the lamella. More recent experiments showed that at high Reynolds numbers the ejecta and lamella are truly distinct jets, but coalesce into a single jet below a threshold in Reynolds number (Zhang *et al.* 2012*a*). At even higher Reynolds numbers multiple generations of ejecta sheets are possible (Zhang *et al.* 2012*b*). The dynamics of the ejecta sheet was also studied by Thoroddsen *et al.* (2011) and Thoraval *et al.* (2012), who reproduced numerically the complex evolution of the ejecta shapes.

Here we report the results of our investigation of the bifurcation from one to two jets using experiments and numerical simulations. We report two different types of experiments. In the first set, the use of different fluids in the drop and the pool allow for the direct observation of the interface between the liquid in the pool and the drop. These reveal that a second jet is formed by a vortex ring separating from the free surface and later resurfacing. In the second set, the fluid is the same in the drop and pool. While the vortex is not experimentally observable in these experiments, the similar shape of the air-liquid interface in both the two-fluid experiments and single-fluid experiments (compare figs. 1(g) and 2(e)) strongly suggests that the same vortex shedding observed directly in the two-fluid system is also occurring in the single-fluid system. This is confirmed by our numerical simulations of the single-fluid system. We observe in simulations a vortex that either remains attached to the surface or separates from the surface depending on the system parameters. When the vortex remains attached a single jet is produced; when it detaches two jets are produced. While we were unable to identify the mechanism causing the transition, we find that the capillary number is the best order parameter for characterizing it.

## 2. Experiments

In the experiments of Zhang *et al.* (2012*a*,*b*) the impact of a drop onto a deep pool of the same liquid was studied using X-ray high speed phase contrast imaging. These

experiments showed the existence of two distinct sheet-like jets, each capable of producing secondary droplets, that at low Reynolds numbers merged into a single jet (see Fig. 1. The earlier emerging of these has the usual characteristics of a jet generated by the collision of fluid bodies. We call this jet the ejecta since it most resembles the ejecta sheet identified by Weiss & Yarin (1999) and Thoroddsen (2002). The later emerging jet begins curled-up and unwinds with time, an evolution so patently different than that of the ejecta that it strongly hints at a different genesis. Here we call this structure the roll jet. At low Reynolds numbers, only one jet is generated and can be interpreted as a merger of the ejecta and the roll jet into a single jet. Here we call this single jet the lamella because it most resembles the structure traditionally identified as the jet that produces a crown (or corona) splash (e.g. fig. 1 of Zhang *et al.* (2010)).

Thoraval *et al.* (2012) showed that the base of the ejecta sheet can rise on the side of the drop shedding vortices along the way. To investigate whether such a vortex is present in conditions similar to those where two jets form, we repeated the experiments described in Zhang *et al.* (2012*a*) except that the fluid in the pool and the drop were slightly different. The fluid in the drop was a silicone oil with density $\rho = 0.759$ g/cm$^3$, viscosity $\mu = 0.49$ cP, and surface tension $\sigma = 15.7$ dyn/cm; the fluid in the pool was also a silicone oil with $\rho = 0.813$ g/cm$^3$, $\mu = 0.82$ cP, and $\sigma = 17.2$ dyn/cm. These two fluids are miscible and as such the interfacial tension between them is negligible. Since X-ray phase contrast imaging is sensitive to density gradients, these experiments reveal the evolution of the fluid-fluid interface between the drop and the pool. A typical sequence illustrating the formation of a rolled up vortex sheet, which we call a roll jet is shown in fig. 2 (see supplemental movie 1 for a video of the same sequence). In frame (a) of this figure, the presence of two vortices is shown inside the two bumps on the side of the drop. The first jet emerges (frame (b)) at the location of the higher vortex. Despite its early emergence, its characteristically curled shape indicates that it is not an ejecta sheet, but rather a roll jet. The second vortex separates from the free surface and forms a second roll jet further from the center (see frames d - f).

## 3. Numerical simulations

The similar morphology of the jets in the two fluid system to those in the single fluid system (drop and pool composed of same fluid) suggests the same vortex dynamics is occurring in a single fluid system. Since the motion of the drop-pool interface is invisible to the X-ray technique when the fluids are the same, we instead used numerical simulations. These reproduce with high fidelity all the features and evolution of the free surface observed experimentally. Moreover, the simulations provide data on the flow everywhere in the fluid and access to a greater swath of the parameter space than is accessible experimentally.

### 3.1. *Numerical method*

We simulate a gas-liquid system with respective densities $\rho_g$ and $\rho_l$ and viscosities $\mu_g$ and $\mu_l$ using the Navier-Stokes equations:

$$\rho(\partial_t \mathbf{u} + \mathbf{u}\cdot\nabla\mathbf{u}) = -\nabla p + \nabla\cdot(2\mu\mathbf{D}) + \gamma\kappa\delta_s\mathbf{n} + \rho g\mathbf{z},$$
$$\nabla\cdot\mathbf{u} = 0.$$

where $\mathbf{u}$ is the fluid velocity, $\rho \equiv \rho(\mathbf{x}, t)$ is the density, $\mu \equiv \mu(\mathbf{x}, t)$ is the viscosity and $\mathbf{D}$ is the deformation tensor. The Dirac distribution function $\delta_s$ expresses the fact that the surface tension term is concentrated at the interface, $\kappa$ and $\mathbf{n}$ being the curvature and the normal of the interface respectively. We use the Gerris code, a quad/octree-based

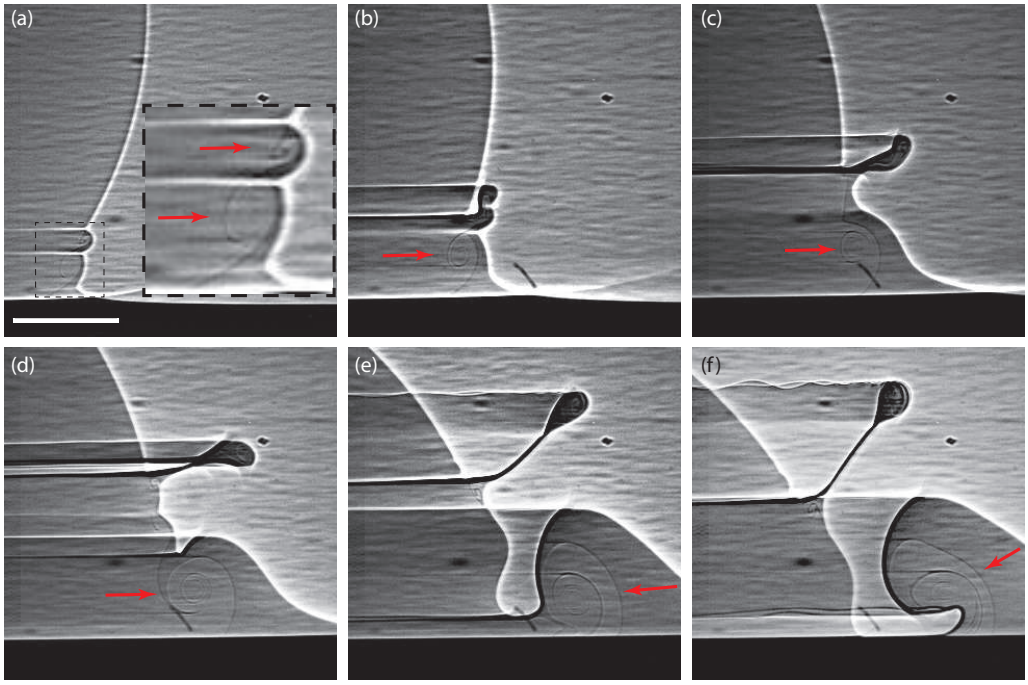


FIGURE 2. Phase contrast X-ray images showing the formation of two roll jets. A vortex forms on the interface near the nascent ejecta (a & b), separates (c), and reconnects with the interface to form the roll jet (d - f). Impact speed $U = 220$ cm/s and drop diameter $D = 0.16$ cm. The scale bar correspond to 0.2 mm. The fluid in the pool and the drop were slightly different (see text). Since our technique is sensitive to density differences, the vortex is rendered visible by the contrast between the entwined fluids. The red arrows points at the center of the vortex.

multilevel solver described in detail in Popinet (2003). The interface is tracked by a volume-of-fluid method described in Popinet (2009); Tryggvason *et al.* (2011). The accuracy of the code has been validated for a number of multiphase flow problems (Agbaglah *et al.* 2011; Fuster *et al.* 2009; Popinet 2009) including splashing (see e.g. Thoraval *et al.* 2012, 2013; Agbaglah & Deegan 2014).

### 3.2. *Numerical simulations*

We model a drop with diameter D and velocity U falling vertically through an initially quiescent gas and impacting on a deep pool of the same liquid with depth H = 5D. The simulation is characterized by five dimensionless parameters: the viscosity and density ratios ($\mu_l/\mu_g$ and $\rho_l/\rho_g$), the liquid Reynolds number $Re = \rho_l \mathrm{UD}/\mu_l$, the Weber number $We = \rho_l \mathrm{U}^2\mathrm{D}/\sigma$, and the Froude number $U^2/(gD)$. In our initial simulations we could discern no effect due to gravity, and thus it was omitted from subsequent simulations. We use the axisymmetric formulation of the Navier-Stokes equations to exploit the symmetry of the experimental features studied here. The computational domain is $5\mathrm{D} \times 10\mathrm{D}$ and is discretized with an adaptive mesh up to a maximum number $2^{14}$ grid points along each dimension, corresponding to a minimum mesh size $\Delta x = \mathrm{D}/3277$. The mesh is adapted based on four criteria: distance to the interface, curvature of the interface, vorticity and velocity magnitude.

Figure 3 compares simulation results with the equivalent experimental profiles obtained by high speed X-ray imaging. The experimental profiles were obtained in the same data runs reported in (Zhang *et al.* 2012*a*). Briefly, the fluid was silicone oil with D = 0.2 cm,

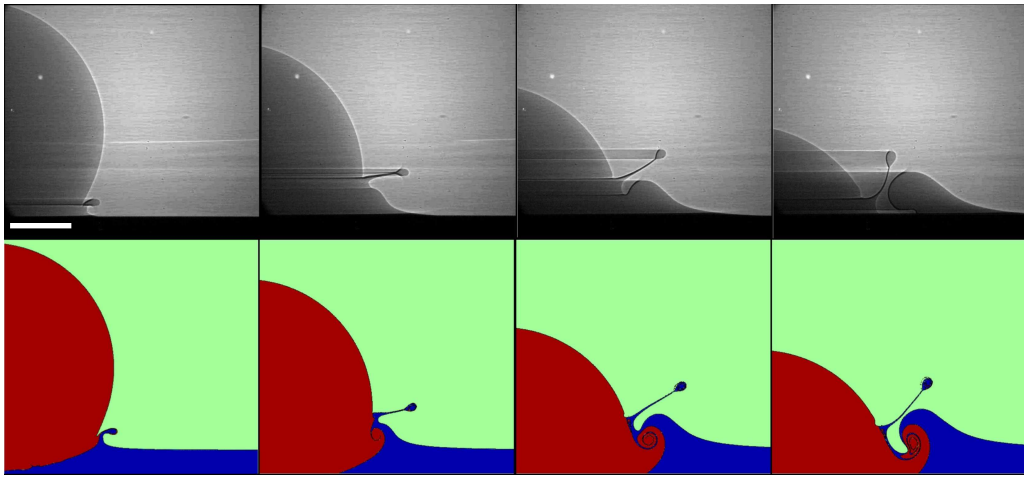

FIGURE 3. Comparison of X-ray phase contrast images from experiments (top) with simulation (bottom) for $We = 292$ and $Re = 2042$ at $\tilde{t} = tU/D = 0.161,\ 0.261,\ 0.46,\ 0.811$ (left to right). Experimental configuration and conditions are given in Zhang *et al.* (2012*a*) for the SO3 fluid listed therein; the scale bar correspond to 0.2 mm. The colors in simulation indicate the fluid from the drop (red) and the pool (blue), and the ambient gas (green).

$\mu_l = 1.3$ cP, $\rho_l = 0.851$ g/cm$^3$, $\sigma = 17.6$ dyne/cm, and $U = 156$ cm/s, incidence was normal to the pool, the surrounding gas was air, and the pool depth was 5 cm. The excellent agreement between the experiments and simulations demonstrate the accuracy with which our simulations capture the dynamics.

We ran simulations in the parameter range $Re \leqslant 5000$ and $We \leqslant 900$ with air as the surrounding gas ($\mu_g = 1.94 \times 10^{-2}$ cP and $\rho_g = 1.2 \times 10^{-3}$ g/cm$^3$). We fixed $\rho_l/\rho_g = 709$, $U = 156$ cm/s, and $D = 0.2$ cm, and varied $\mu_l$ and $\sigma$ to select $Re$ and $We$. We observe the four distinct behaviors shown in fig. 4. At high $Re$ where two-jets emerge, the simulation results in fig. 4 (c) show a vortex ring driving the growth of the roll jet. This vortex ring originates at the corner where the ejecta and the drop meet, it detaches from the free surface along the downward direction, travels horizontal below the pool level, and resurfaces to form the roll jet. Figure 5 illustrates the flow field around the vortex shedding event and shows that after the vortex sheds all the fluid entering the ejecta comes from the pool.

Irrespective of $Re$, at early times there is always a large patch of vorticity near the point where the upper side of the jet and the drop meet. The large outward mean flow hides that this vorticity patch is a vortex attached to the free surface (see for example Fig.5). Below some critical $Re$ (see fig. 4 (b)) we observe that the vortex ring remains attached to the interface at all times, becoming progressively larger but weaker, and eventually merges with the base of the ejecta to form the lamella. Thus our simulations show that the transition from one jet (the lamella) to two jets (an ejecta and a roll jet) observed in experiments (Zhang *et al.* 2012*a*) is dictated by whether the vortex remains attached to the free surface.

At the highest $Re$ and $We$ in our range of study the ejecta reconnects with the drop surface capturing a bubble. This process leads to air-entrainment and vortex separation as shown in fig. 4(d) and is the same as the "bumping" regime described in Thoraval *et al.* (2012). At high $Re$ and low $We$ we observe vortex shedding and the formation of a lamella but no ejecta.

The parametric dependence of the four regimes depicted in fig. 4 as found in simula-

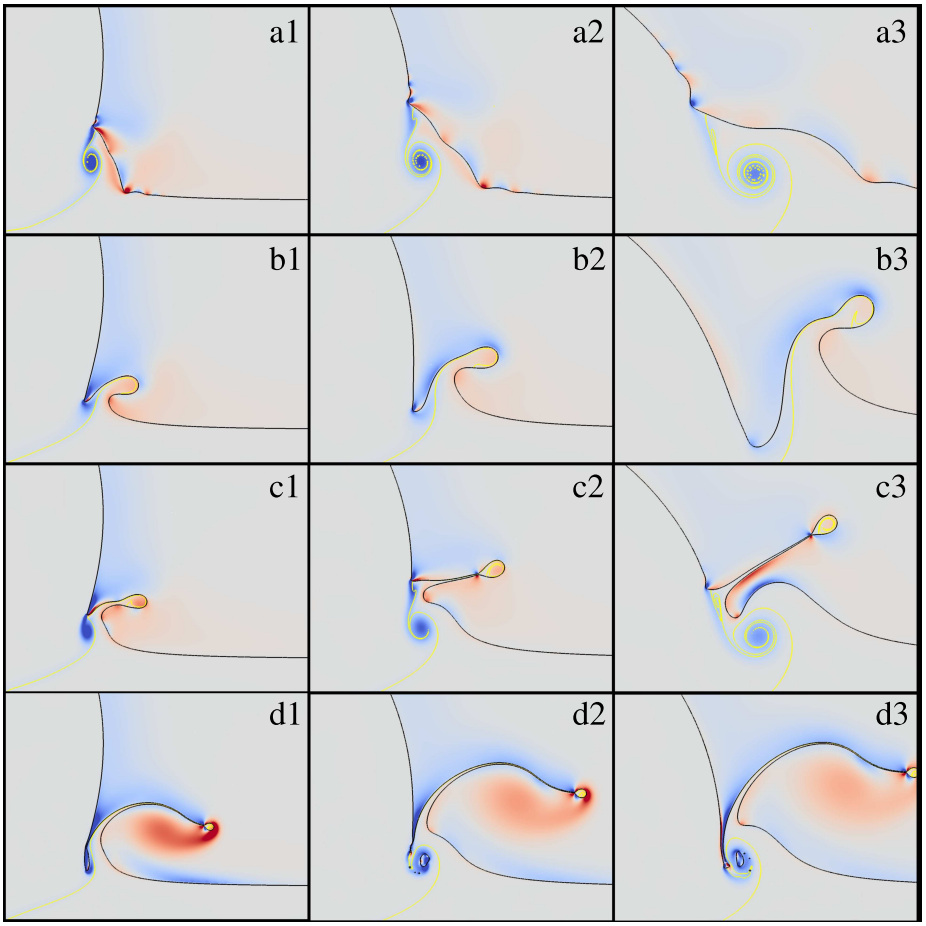


FIGURE 4. Qualitatively different flows observed in simulations: (a) vortex separation forming a roll jet without a preceding ejecta ($We = 100, Re = 2500$); (b) ejecta without vortex shedding leading to a lamella ($We = 292, Re = 1000$); (c) ejecta plus vortex separation leading to separate roll jet ($We = 292, Re = 2042$); (d) collision of the ejecta with the drop plus vortex shedding leading to a separate roll jet ($We = 700, Re = 3000$). Columns correspond to equal times $\tilde{t} = 0.211, 0.311, 0.511$ (from left to right) except for (d3) which corresponds to $\tilde{t} = 0.372$. The color indicates vorticity with blue/red representing counterclockwise/clockwise rotation. The thin yellow line within the drop indicates the boundary between the fluid from the drop and the pool.

tions is given by the phase diagram in fig. 6. Each simulation point in fig. 6 took two weeks of computation on seven cores using the MPI library combined with the dynamic load-balancing as described in Agbaglah *et al.* (2011). For reference the equivalent experimental observations from Zhang *et al.* (2012*a*) are also shown. The two datasets show strong agreement. The boundary between the shedding and no shedding is reasonably captured by the relation $Re = 5\,We$ or equivalently $Ca \equiv \eta U/\sigma = 0.2$.

### 3.3. *Characterizing the vortex shedding*

In order to investigate the mechanism for vortex shedding, we measured various characteristics of the flow. Since the shedding event occurs in the vicinity where the jet emerges from the drop, our measurements focused on this zone and particularly on **T** the point within this zone of maximum curvature of the air-liquid interface (see fig. 5(a)). We

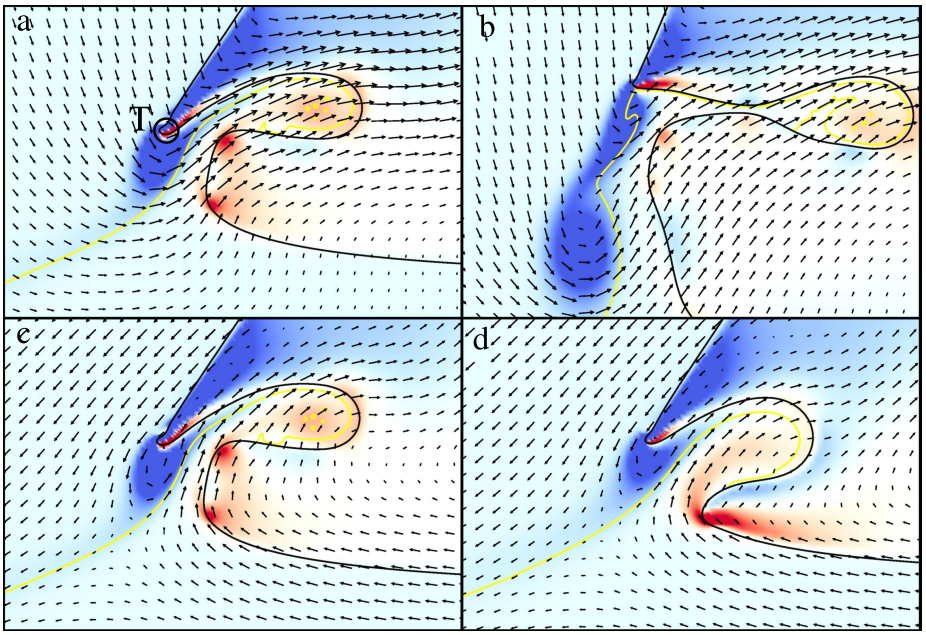


FIGURE 5. Flow field and vorticity at the base of the jet in the lab frame (a, b) and in the reference frame comoving with the point **T** (c,d). (a-c) Vortex shedding splash at $We = 292$ and $Re = 3000$ for $\tilde{t} = 0.141$ (a, c) and $\tilde{t} = 0.236$ (b). Note that in (b) the liquid entering the jet originates almost exclusively from the pool. (d) Non-shedding splash at $We = 292$ and $Re = 1500$ for $\tilde{t} = 0.141$. The flow field of non-shedding splashes at other parameter values at all times looks similar to (a) in the lab frame or (c or d ) in comoving frame.

found that there is no simple characteristics that heralds a shedding event. For example, as shown in fig. 7 the time dependence and magnitude of the curvature $\kappa_T$ at **T** right up until the shedding event begins are indistinguishable from those of the non-shedding cases. In other words, we find no way to predict which configurations will shed a vortex. The same is true of the vorticity (see fig. 8), the velocity (see remark in fig. 5), the local Reynolds number $Re_L = \rho_l u \kappa_T^{-1}/\mu_l$ (see fig. 9(a)) where $u$ is the maximum speed tangential to the interface around **T**, and the local Weber number $\rho_l u^2 \kappa_T^{-1}/\sigma$ .

Nonetheless, the initiation of shedding is clearly signaled by the vorticity and the curvature. Figure 7(b) shows that a subset of the simulations exhibit a minima in the curvature. All shedding cases exhibit such a minima and the minima occurs prior to a visually discernible separation of the vortex. Thus we take this minima as a signal that the vortex separation process has started. Rescaling the time by the visco-capillary time $t_{\mu\sigma} = \mu_l D/\sigma$ as in fig. 7(b) shows that the initiation of shedding occurs at a remarkable uniform time $t \approx 1.05 t_{\mu\sigma}$. These results hint at the importance of the Capillary number $Ca = \mu_l U/\sigma$ because $t_{\mu\sigma}$ in dimensionless units $D/U$ is $Ca$. Indeed, the local capillary number $Ca_L = u\mu_l/\sigma$ for vortex-shedding splashes are lower at all times than for non-shedding splashes (see fig. 9(b)). Moreover, taking the time averaging threshold value of $Ca$ indicated in fig. 9(b) yields a value of 0.2. Plotting this value on the phase diagram (fig. 6) fairly accurately captures the transition. Therefore, our data indicates that understanding the interplay between viscous and capillary forces in the vicinity of **T** is the most important ingredient for understanding the transition between one and two jets.

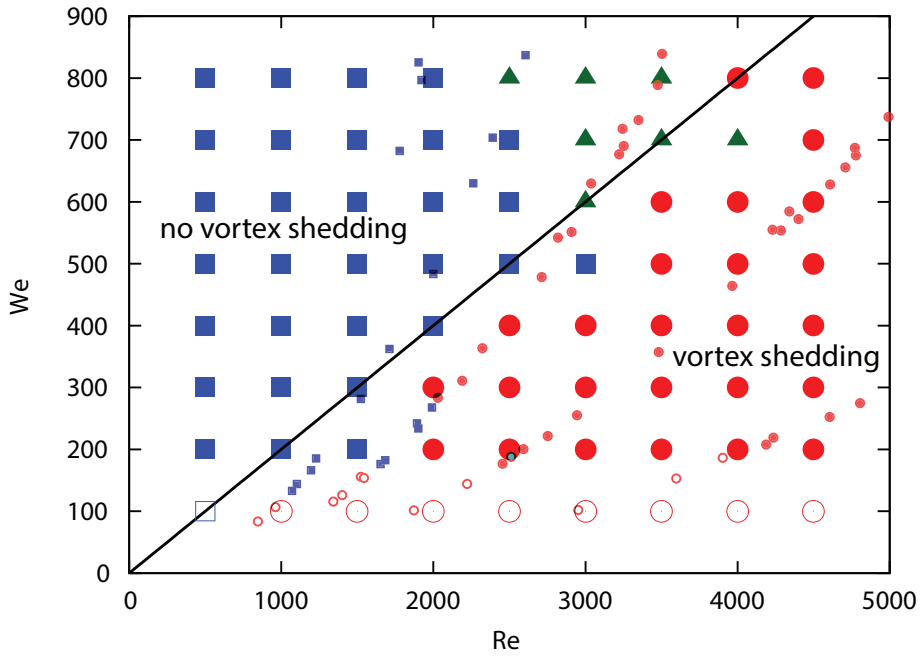


FIGURE 6. Phase diagram for vortex shedding. Simulations (shown with large symbols) which exhibit vortex shedding are represented with circles, no vortex shedding with squares, and bumping with triangles. Filled symbols indicate presence of ejecta while open symbols have no ejecta. Experimental results reported in Zhang *et al.* (2012*a*) are plotted with small symbols using the same convention as for the simulations; the bumping regime was not distinguished in those experiments. The solid dark line represents the approximate limit of the vorticity shedding regime: $Ca = 0.2$.

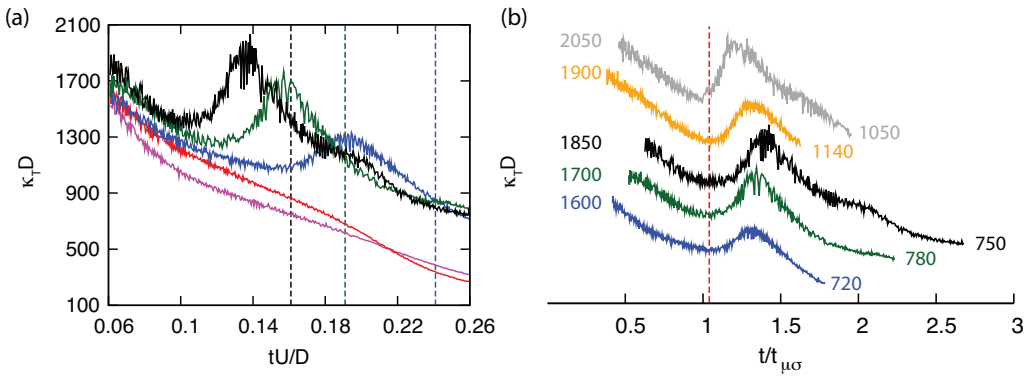


FIGURE 7. (a) Mean curvature at **T** versus time for $We = 300$ and $Re = 1000$ (magenta), 1500 (red), 2000 (blue), 2500 (dark-green) and 3000 (black). The vertical dashed lines indicate the time of the vortex separation chosen by eye when the material line defined by the pool-drop interface exhibited strong swirling such as in fig. 4(c2). The peak in the data indicates vortex shedding; conversely, its absence indicates the vortex remains attached to the interface. (b) Mean curvature at **T** with a time in units of the visco-capillary time ($t_{\mu\sigma} = \mu_l D/\sigma$) for $We = 300$ and $Re = 2000$ (blue), 2500 (dark-green), 3000 (black) and $We = 400$ and $Re = 2500$ (orange), 3000 (dark-gray). The curves have been vertically shifted in order to avoid overlapping and clearly show the position of the minima; their starting and ending values are listed with the same color as the data.

## 4. Discussion and Conclusion

We used experiments and numerical simulations to observe the transition from one jet to two jets in splashing from impact of a drop on a deep pool of the same liquid as a function of $Re$ and $We$. We find that the mechanism driving this transition is the separation of a ring vortex from the air-liquid interface where the first jet emerges from the drop. The separated vortex eventually resurfaces and forms a second jet. The character of this second jet is quite distinct from that of the first jet. The first jet is formed through collision: two bodies of fluid collide and their linear momentum is focused into an outwardbound stream. In contrast, the second jet emerges tightly wound, uncoiling as it evolves whipping the fluid at its tip outward.

In our experiments we focused on the a deep pool because a shallower pool introduces another parameter, the depth, and the additional complexity that entails (Yarin & Weiss 1995; Cossali *et al.* 1997; Wang & Chen 2000; Rioboo *et al.* 2003). Nonetheless, the limited depth-wise penetration of the flow observed in simulations (see Fig. 4) suggests that depths as shallow as $D$ are sufficient for the manifestation of two jets. The observation of vortex shedding at the pool-drop interface (Castrejón-Pita *et al.* 2012) for $\tilde{t} < 1$ and in shallower pool depths Thoraval *et al.* (2013) suggest that similar phenomena may occur in yet shallower depths at high $Re$.

Our simulations show that the transition is best characterized by the capillary number. Nonetheless, the separation process sufficiently resembles separation from a free surface observed in other configurations to warrant investigating if the criteria established in these other flows can be usefully applied to splashing. Batchelor (1967) argues on general grounds that separation can only occur at large curvatures. This qualitative statement was examined recently by Moore *et al.* (2014) who looked at the high-Re perturbations to steady two-dimension Helmholtz flows relevant for the flow in the jet root of Wagner's theory for droplet impact (Howison *et al.* 2005). They showed in this situation that vortex shedding is possible only if the $Re_L$ is of order unity. This is consistent with figure 9(a), although unsteady effects could play a role here. Figure 7 shows that the curvature of shedding and non-shedding splashes are comparable, and furthermore the curvature at the instant of shedding is always lower than the values at early times in non-shedding splashes. Hence, the curvature by itself cannot be the sole criteria for shedding.

Leal (1989) investigated separation from a bubble and found that separation occurs when the surface vorticity reaches a critical value and $Re$ is large. As with the curvature, we observe higher surface vorticities in non-shedding splashes than we do at the instant of separation in shedding splashes. Hence, surface vorticity is not a good criteria for vortex shedding in drop impact.

Finally, we note that the flow at **T** resembles the classic problem of a jet plunging into a pool. In the latter, the jet drags the interface downward and for sufficiently fast flows can cause opposing sides of the interface to meet, pinch-off and entrain bubbles. The transition to air entrainment is known to be governed by the local capillary number at low viscosities (Kiger & Duncan 2012). The similar kinematics and the same dependence on the capillary number suggests that physics of the plunging jet may be fruitfully applied to the jet problem considered here.

## 5. Acknowledgements

The authors thank the James S. McDonnell Foundation for support through a 21st Century Science Initiative in Studying Complex Systems Research Award, and S. Weiss

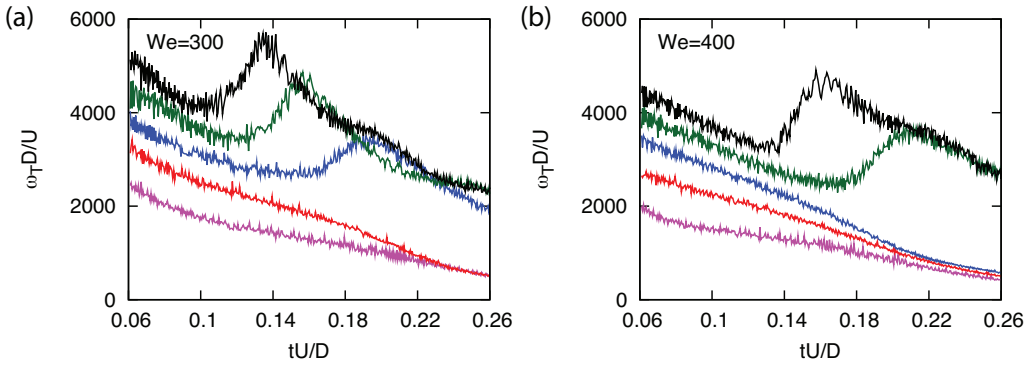


FIGURE 8. Maximum absolute value of the vorticity $\omega_T$ on the interface near **T** (equivalent to the deepest blue in fig. 5) for (a) $We = 300$ and (b) $We = 400$ at $Re = 1000$ (magenta), 1500 (red), 2000 (blue), 2500 (green), 3000 (black).

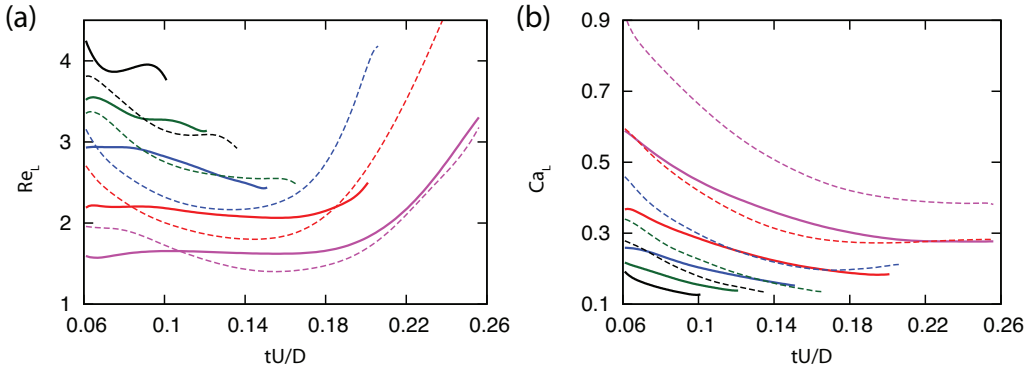


FIGURE 9. (a) Local Reynolds number $Re_L$ and (b) local Capillary number $Ca_L$ around **T** for $We = 300$ (solid) and $We = 400$ (dashed), and $Re = 1000$ (magenta), 1500 (red), 2000 (blue), 2500 (dark-green) and 3000 (black).

and J. Soundar Jerome for valuable discussions, and Claudio Falcón for assistance with the experiments.

## REFERENCES

AGBAGLAH, G. & DEEGAN, R. D. 2014 Growth and instability of the liquid rim in the crown splash regime. *Journal of Fluid Mechanics* **752**, 485–496.

AGBAGLAH, G., DELAUX, S., FUSTER, D., HOEPFFNER, J., JOSSERAND, C., POPINET, S. RAY, P., SCARDOVELLI, R. & ZALESKI, S. 2011 Parallel simulation of multiphase flows using octree adaptivity and the volume-of-fluid method. *Comptes Rendus Mecanique* **339**, 194–207.

BATCHELOR, G. K. 1967 An introduction to fluid dynamics. *Cambridge University Press* .

CASTREJÓN-PITA, A., CASTREJÓN-PITA, J. & HUTCHINGS, I. 2012 Experimental observation of von kármán vortices during drop impact. *Physical Review E* **86**, 045301.

COSSALI, G. E., COGHE, A. & MARENGO, M. 1997 Impact of a single drop on a wetted solid surface. *Experiments in Fluids* **22** (6), 463–472.

DEEGAN, R. D., BRUNET, P. & EGGERS, J. 2008 Complexities of splashing. *Nonlinearity* **21** (1), C1–C11.

FEZZAA, K. & WANG, Y. J. 2008 Ultrafast x-ray phase-contrast imaging of the initial coalescence phase of two water droplets. *Physical Review Letters* **100** (10), 104501.

FUSTER, D., AGBAGLAH, G., JOSSERAND, C., POPINET, S. & ZALESKI, S. 2009 Numerical

simulation of droplets, bubbles and waves: state of the art. *Fluid Dynamics Research* **41** (6), 065001.

Howison, S. D., Ockendon, J. R., Oliver, J. M., Purvis, R. & Smith, F. T. 2005 Droplet impact on a thin fluid layer. *Journal of Fluid Mechanics* **542**, 1–23.

Josserand, C. & Zaleski, S. 2003 Droplet splashing on a thin liquid film. *Physics of Fluids* **15** (6), 1650–1657.

Kiger, K. T. & Duncan, J. H. 2012 Air-entrainment mechanisms in plunging jets and breaking waves. *Annu. Rev. Fluid Mech.* **44**, 563–596.

Kolinski, J. M., Rubinstein, S. M., Mandre, S., Brenner, M. P., Weitz, D. A. & Mahadevan, L. 2012 Skating on a film of air: Drops impacting on a surface. *Physical Review Letters* **108**, 074503.

Leal, L. G. 1989 Vorticity transport and wake structure for bluff bodies at finite reynolds number. *Phys. Fluids* **A 1**, 124–131.

Moore, M. R., Ockendon, H., Ockendon, J. R. & Oliver, J. M. 2014 Capillary and viscous perturbations to helmholtz flows. *Journal of Fluid Mechanics* **742**, R1–R1.

Oguz, H. N. & Prosperetti, A. 1989 Surface-tension effects in the contact of liquid surfaces. *Journal of Fluid Mechanics* **203**, 149–171.

Popinet, S. 2003 Gerris: a tree-based adaptive solver for the incompressible euler equations in complex geometries. *Journal of Computational Physics* **190** (2), 572–600.

Popinet, S. 2009 An accurate adaptive solver for surface-tension-driven interfacial flows. *Journal of Computational Physics* **228** (16), 5838–5866.

Rioboo, R., Bauthier, C., Conti, J., Voue, M. & De Coninck, J. 2003 Experimental investigation of splash and crown formation during single drop impact on wetted surfaces. *Experiments in Fluids* **35** (6), 648–652.

Thoraval, M.-J., Takehara, K., Etoh, T. G., Popinet, S., Ray, P., Josserand, C., Zaleski, S. & Thoroddsen, S. T. 2012 von karman vortex street within an impacting drop. *Physical Review Letters* **108** (26), 264506.

Thoraval, M.-J., Takehara, K., Etoh, T. G. & Thoroddsen, S. T. 2013 Drop impact entrapment of bubble rings. *Journal of Fluid Mechanics* **724**, 234–258.

Thoroddsen, S. T. 2002 The ejecta sheet generated by the impact of a drop. *Journal of Fluid Mechanics* **451**, 373–381.

Thoroddsen, S. T., Etoh, T. G. & Takehara, K. 2003 Air entrapment under an impacting drop. *Journal of Fluid Mechanics* **478**, 125–134.

Thoroddsen, S. T., Thoraval, M. J., Takehara, K. & Etoh, T. G. 2011 Droplet splashing by a slingshot mechanism. *Physical Review Letters* **106** (3).

Tryggvason, G., Scardovelli, R. & Zaleski, S. 2011 *Direct Numerical Simulations of Gas–Liquid Multiphase Flows*. Cambridge University Press.

Wang, A. B. & Chen, C. C. 2000 Splashing impact of a single drop onto very thin liquid films. *Physics Of Fluids* **12** (9), 2155–2158.

Weiss, D. A. & Yarin, A. L. 1999 Single drop impact onto liquid films: neck distortion, jetting, tiny bubble entrainment, and crown formation. *Journal of Fluid Mechanics* **385**, 229–254.

Worthington, A. M. 1882 On impact with a liquid surface. *Proc. Phys. Soc. London* **34**, 217–230.

Xu, L., Zhang, W. W. & Nagel, S. R. 2005 Drop splashing on a dry smooth surface. *Physical Review Letters* **94**, 184505.

Yarin, A. L. 2006 Drop impact dynamics: Splashing, spreading, receding, bouncing. *Annual Review of Fluid Mechanics* **38**, 159–192.

Yarin, A. L. & Weiss, D. A. 1995 Impact of drops on solid-surfaces - self-similar capillary waves, and splashing as a new-type of kinematic discontinuity. *Journal of Fluid Mechanics* **283**, 141–173.

Zhang, L. V., Brunet, P., Eggers, J. & Deegan, R. D. 2010 Wavelength selection in the crown splash. *Physics Of Fluids* **22** (12), 122105.

Zhang, L. V., Toole, J., Fezzaa, K. & Deegan, R. D. 2012*a* Evolution of the ejecta sheet from the impact of a drop with a deep pool. *Journal Of Fluid Mechanics* **690**, 5–15.

Zhang, L. V., Toole, J., Fezzaa, K. & Deegan, R. D. 2012*b* Splashing from drop impact into a deep pool: multiplicity of jets and the failure of conventional scaling. *Journal of Fluid Mechanics* **703**, 402–413.